Fuel Processing Technology 119 (2014) 245–255

Contents lists available at ScienceDirect

Fuel Processing Technology

journal homepage: www.elsevier.com/locate/fuproc

Exergetic analysis of a fast pyrolysis process for bio-oil production

Jens F. Peters [a,*], Fontina Petrakopoulou [b,c], Javier Dufour [a,d]

[a] Systems Analysis Unit, Instituto IMDEA Energía, Móstoles 28935 Spain
[b] Unit of Environmental Science and Technology, National Technical University of Athens, Athens 15773, Greece
[c] School of Production Engineering and Management, Technical University of Crete, Chania 73100, Greece
[d] Department of Chemical and Energy Technology, Rey Juan Carlos University, Móstoles 28933, Spain

ARTICLE INFO

Article history:
Received 25 June 2013
Received in revised form 25 October 2013
Accepted 13 November 2013
Available online 7 December 2013

Keywords:
Biomass
Bio-oil
Exergetic analysis
Exergetic efficiency
Fast pyrolysis

ABSTRACT

This paper presents an exergetic analysis of a fast pyrolysis plant simulated in Aspen Plus, producing crude bio-oil from lignocellulosic feedstock (hybrid poplar woodchips). The simulation includes the drying and pretreatment of the biomass, the pyrolysis reactor, product recovery, and a combustion reactor that provides the process heat. Chemical and physical exergies are determined for all process streams and the exergy destruction is calculated at the component level of the plant. The overall exergetic efficiency of the plant is found to be 71.2%, with the gas-and-char combustor of the plant causing the highest exergy destruction. Relatively high irreversibilities are also calculated in the pyrolysis reactor and the bio-oil recovery section (quench and water cooler), as well as in the dryer and the mill. Further investigation shows considerable potential for improvement when introducing the hot exhaust gases of the combustor directly in the dryer without using part of their thermal energy for preheating the combustion air. This measure increases the overall plant efficiency to 73.2% by reducing the inefficiencies in the dryer and the heat exchangers. Lastly, the contribution of the compressors and pumps to the overall exergy destruction is found to be rather small.

1. Introduction

Biomass energy is considered a central pillar in strategies for reducing future dependency on fossil fuels and greenhouse gas (GHG) emissions. This is also reflected in policy decisions, such as the Renewable Energy Directive of the European Union [1], which sets a target of 20% renewable energy contribution by 2020, including a 10% share of biofuels. However, biomass has the important drawback of being a heterogeneous solid fuel with a relatively low density. This complicates the handling and transport processes, limiting, thereby, the potential for industrial applications. One possibility to overcome this problem is to convert the biomass into bio-oil through fast pyrolysis. The generated bio-oil has a similar heating value, but a higher density and is, as a liquid, easier to handle [2].

Pyrolysis is the thermal decomposition of a carbonaceous feedstock in a non-oxidative atmosphere that yields gases, chars and condensable vapors (tarry liquids, the bio-oil). Fast heating, short residence times and temperatures around 500 °C (fast pyrolysis) maximize the liquid yields from the pyrolysis of the biomass. The resulting yields of the fractions and their composition depend on the feedstock and the operational conditions of the process and are in average 15% gas, 15% chars and 70% liquids [3,4].

On-going research in energy applications of bio-oil obtained from biomass pyrolysis include co-combustion in natural gas power plants [5], direct combustion in stationary diesel engines [6,7] and upgrading to a high-quality engine fuel for vehicles [8–10]. An extensive review on the current activities in the field was recently published by Meier et al. [11]. However, only very few commercial energy applications for bio-oil exist up-to-date [11,12]. In order for the bio-oil to become competitive with fossil fuels, pyrolysis processes have to become as efficient as possible. Exergetic analysis is a powerful tool for optimizing energy conversion processes.

Exergetic analysis is a methodology that detects thermodynamic irreversibilities in energy conversion systems and can be used to maximize the operational efficiency. Based on the second law of thermodynamics, exergy represents the quality of energy, i.e., its maximum capability to generate work when bringing a system into equilibrium with its environment. In this way, an exergetic analysis permits the identification of the useful part of energy and pinpoints thermodynamic inefficiencies that a conventional energy analysis cannot detect [13,14].

To date, only a few publications exist on the thermodynamic performance of pyrolysis plants. To the best of the authors' knowledge, one study on the exergetic analysis of a fast pyrolysis plant has been published by Boateng et al. [15], while Kalinci et al. [16] included pyrolysis as a sub-process in their assessment of a gasification system.

The present article presents the simulation and exergetic analysis of a pyrolysis plant that produces bio-oil from lignocellulosic hybrid poplar feedstock. Using the results of the analysis, we identify the main exergetic inefficiencies of the plant and discuss ways to improve the operating efficiency of the process. The potential for improvement of specific components/processes in an energy conversion system can only be

* Corresponding author at: Systems Analysis Unit, Instituto IMDEA Energía 28933 Móstoles, Madrid, Spain
E-mail address: jens.peters@imdea.org (J.F. Peters).

0378-3820/$ – see front matter © 2013 Elsevier B.V. All rights reserved.
http://dx.doi.org/10.1016/j.fuproc.2013.11.007

quantified using advanced exergy-based methods [17,18]. Here, we use the results of conventional exergetic analysis in an effort to improve the operation of the presented energy conversion system by modifying components with relatively high irreversibilities.

2. Process simulation

Thermodynamic data necessary for the exergetic analysis are obtained from the simulation of the process in Aspen Plus. While Aspen Plus is commercial software originally developed for the petrochemical industry for the simulation of chemical processes, it is also often used for the simulation of power plants. It is equipped with a large database of chemical compounds and a property estimation system for calculating stream properties and chemical reactions. Nevertheless, unconventional compounds like biomass or pyrolysis products are not included in the database and the corresponding properties and reaction mechanisms must be defined by the user manually.

This work presents the simulation of a fast pyrolysis plant producing bio-oil with integrated reaction mechanisms, the corresponding properties of the model compounds and the stream tables obtained and used as basis for an exergetic analysis. The biomass used in the simulation is assumed to be composed of cellulose, hemicellulose and lignin, ash, water and some N, S and Cl-containing compounds. Extractives and other substances are not considered and their fate during the pyrolysis reactions can therefore not be calculated.

The chosen configuration of the plant agrees with current existing industrial plants and existing publications on the topic [19–22]. Fig. 1 shows the flow diagram of the pyrolysis plant, which is divided into three sections: the pre-treatment (PTR), the pyrolysis (PYR) and the gas-and-char combustor (GCC) sections. This flow diagram allows the identification of all streams used in the assessment of the plant and may be used to reconstruct its configuration completely. The simulated components of the different sections of the plant are described below.

2.1. Pre-treatment section (PTR)

Lignocellulosic biomass (hybrid poplar with 50%$_{wt}$ water content; Stream 86 in Fig. 1) is dried in a direct-contact dryer (DRYREACT) to a water content of 7%$_{wt}$ using thermal energy from the hot exhaust gases (Stream 18) exiting the GCC Reactor. An electric hammer mill (BMMILL), followed by a sieve (BMSIEVE; hole size 3 mm) reduces the particle size of the dry feedstock (Stream 3) to 3 mm (Stream 8), as required by the subsequent pyrolysis reactor [23]. For calculating the required mill power, Aspen Plus requires the hardgrove grindability index of the processed solids, a unit commonly used for measuring the grindability of fossil coals (high grindability values characterize brittle and easily grindable coals). For this work, the grindability index of the biomass was set to four, to provide the grinding energy consumption in accordance with the work of Jones et al. [19] and Mani [24]. The hot dry wood (Streams 9 and 10) is cooled down to a temperature close to 50 °C on the conveyor belts (represented by BMCOOLR) before it enters the pyrolysis section of the plant. The electricity consumption of the mill is included in the analysis, while that of the conveyor belts and the feeder screws is neglected.

2.2. Pyrolysis (PYR)

In the pyrolysis section the dry and ground biomass (Stream 23) is decomposed into bio-oil, char and gas and the pyrolysis products are recovered and separated.

2.2.1. Pyrolysis reactor configuration

The pyrolysis reactor is a circulating fluid-bed (CFB) reactor with a sand bed operating at 520 °C [25]. The reactor bed is fluidized by recirculated pyrolysis gases (Stream 38) with a mass flow 1.5 times higher than that of the biomass feed, resulting in an average bed residence time of the particles of 2 s and a vapor residence time of 0.5 s [19]. The sand also acts as a heat carrier. After separating the sand and the char from the hot pyrolysis vapors in a series of hot cyclones, the sand is sent to the GCC, it is heated up to the temperature of the pyrolysis process, and sent back to the reactor (Stream 50/51). The remaining char, not separated in the cyclone or deposited on the sand particles, is burned in the GCC as well. The unit "PY-Reactor" (Fig. 1) contains three reactors (1BMDECMP, 1CSTIR, 1SLWYLD), described in more detail below, the sand bed heat exchanger (PYSANDHX), the flue gas mixer (1BBMIX), and the hot cyclone (PYCHRCYC). For the purpose of the analysis presented here, and since these components are inseparable parts of a CFB pyrolysis reactor, they are treated as one single component.

2.2.2. Pyrolysis reaction model

The pyrolysis yields and products are calculated based on a kinetic reaction model, which, under given reactor conditions, permits the simulation of the pyrolysis process of any lignocellulosic biomass [26]. A two-stage reaction model accounts for the primary, as well as for the complex secondary pyrolysis reactions. The produced bio-oil is modeled with a high level of detail (33 components including organic acids, aldehydes, alcohols, ketenes, phenols, sugar derivatives and degraded lignin) and the char with a realistic atomic composition. Validation

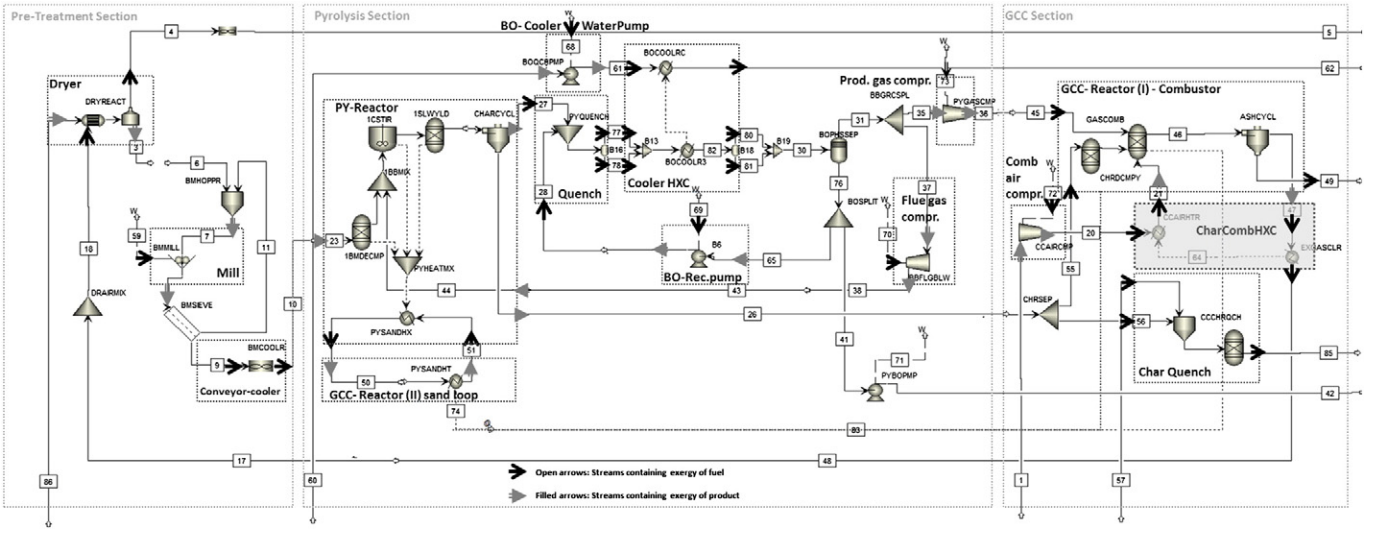

Fig. 1. Plant flowsheet; the process units examined in the exergetic analysis are indicated by dotted boxes.

tests show that the model is able to calculate product composition and yields with a good precision for a pyrolysis temperature range of 450–650 °C and residence times of 0.5–2500 s [26]. As the modeling of the complex pyrolysis reactions in Aspen Plus is not possible with just one reactor, three reactors (1BMDECMP, 1CSTIR, 1SLWYLD) are used to simulate the intermediate stages of reactions occurring within a single real pyrolysis reactor.

Decomposition reactions: In the first – RYield type – reactor (1BMDECMP), the biomass feedstock (a nonconventional compound defined by its atomic composition) is decomposed into its principal building blocks (cellulose, lignin and hemicellulose), as required by the subsequent second pyrolysis reactor. The products of the decomposition reactor are xylan–as hemicellulose monomer–, the cellulose monomer $C_6H_{10}O_5$, and seven lignin fragment monomers with different C, H and O contents. While cellulose and hemicellulose are compounds with rather fixed monomer structure, lignin is more heterogeneous and can give a wide range of different monomers when decomposing. The amount of each of the seven lignin monomers released depends on the initial biomass composition.

Primary pyrolysis reactions: In the second – RCStir-type – reactor (1CSTIR), a kinetic reaction model based on the work of Ranzi et al., Faravelli et al., Calonaci et al., and Dupont et al. [27–30] is implemented for the primary pyrolysis reactions. Using the decomposition monomer compounds from the 1BMDECMP reactor, the principal pyrolysis products are calculated via the implementation of over 150 individual kinetic reactions. Hence, the yields and the composition of the pyrolysis products of a given feedstock depend on reactor temperature and residence time.

Secondary pyrolysis reactions: For the heterogeneous vapor-phase reactions (secondary condensation and polymerization), no kinetic modeling is possible due to lack of knowledge about the mechanisms of these highly complex reactions. These reactions are implemented in an RYield reactor (1SLWYLD) using a linear regression algorithm that adjusts the fractional yields according to the mechanisms presented in the work of Hoekstra et al. [31].

Calculated pyrolysis products: In this work, reactor conditions similar to the ones used by Jones et al. [19] are used, fast pyrolysis at 520 °C with 2 s of bed residence time and 0.5 s of vapor residence time. The yields obtained under these conditions for the given hybrid poplar wood with 7% moisture (after drying) are 13.4% gas (Stream 77), 68.9% oil (Stream 78) and 17.7% char (Stream 28). These results agree well with experimental data [26]. The detailed composition of the product streams can be found in the Appendix of the paper.

2.2.3. Product recovery

The pyrolysis products that leave the PY-Reactor unit pass a series of cyclones (CHARCYCL) to separate the chars (Stream 26). The remaining vapors (Stream 27) are then rapidly quenched in PYQUENCH with recirculated cold bio-oil (Streams 28 and 65) to stop the secondary decomposition and polymerization reactions, which would reduce liquid yields. The fraction of the bio-oil recirculated to the quench by the BO-Recycle-Pump (B6) is adjusted by a design specification (separator BOSPLIT) in order to achieve a quench outlet temperature of 62 °C. Although the quench cooling is thermodynamically unfavorable, it is necessary to avoid fouling and heat exchanger failure [32]. To maximize liquid recovery, the quench products (Streams 77 & 78; representing the gas and liquid fractions of the stream) are cooled to 27 °C in the water-cooler BOCOOLR3. The cooling water is driven by the BO-Cooler Water Pump (BOQCHMP) (Streams 60 and 61). A flash unit (BOPHSSEP) separates the incondensable pyrolysis gas (Stream 31) from the condensed liquids (Stream 76) that constitute the bio-oil product of the plant (Stream 42). The gas fraction is split in BBGRCSPL into a flue gas fraction (Stream 37), which is pressurized by the flue gas compressor (BBFLGBLW) and recirculated to the PY-Reactor for fluidizing the reactor bed (Stream 38/43), and a product gas fraction (Stream 35), which is pressurized in the product gas compressor (PYGASCMP) and is combusted in the GCC-Reactor (Stream 36). The sand cycle (Streams 50 and 51) transfers the heat from the GCC-Reactor to the PY-Reactor.

2.3. Gas-and-char combustor (GCC)

In the GCC section the pyrolysis gases and a fraction of the char are combusted to provide process heat to the PYR section.

2.3.1. GCC reactor configuration

Similar to the PY-Reactor unit in the PYR-section, the GCC-Reactor unit consists of several components: two reactors and a cyclone. An RYield reactor (CHRDCMPY) that decomposes the char into its atomic composition and an RGibbs reactor (GASCOMB) that calculates the reaction products through the minimization of the Gibbs free energy. The combustion products leave the GCC-Reactor after passing a series of hot cyclones (ASHCYCL), which separate the ashes (Stream 49) from the hot exhaust gases (Stream 46). The combustion heat (Stream 74 / 83) is transferred to the sand loop (Streams 50 and 51) by PYSANDHT and from there to the pyrolysis reactor (PYSANDHX).

2.3.2. Heat requirements of biomass drying

The hot exhaust gases are recirculated from the combustor to the PTR section in order to provide the process heat for drying the biomass. The GCC-Reactor operates at 1.7 bar accounting for pressure drops within both the BM-Dryer and the components that precede it (0.3 bar in the heat exchanger and 0.2 bar in the dryer; see complete stream tables in the Appendix). Hence, the combustion air (Stream 1) is compressed to 2 bar in the compressor CCAIRCMP (Stream 20) before it is preheated (Stream 21) in the CharCombHXC (CCAIRHTR and EXGASCLR) by the exhaust gases (Streams 47 and 48) that are consequently cooled down to 327 °C. A design specification is used to regulate the air flow, in order to maintain an exhaust gas flow high enough to dry the biomass to the required moisture. The flow of the combustion air is, hence, not determined by the stoichiometric oxygen demand of the combustion reaction but by the mass flow of the exhaust gas required in the BM-Dryer.

2.3.3. Char combustion

A char splitter (CHRSEP) regulates the fraction of the char (coming from the PYR section, Stream 26) needed in the combustion process in the GCC-Reactor (Stream 55). The fraction of the char burned is controlled by a design specification assuring that the required amount of process heat is generated. No heat export or co-generation of electricity has been considered, since the aim of this work is an assessment of the pyrolysis process only. Assuming char combustion for other purposes would inevitably increase the inefficiencies of the overall process and hence skew the results. The surplus char that is not burned (Stream 56) is quenched with water (Stream 57) in the Char Quench (CCCHRQCH) to avoid auto-ignition and to facilitate further handling (the pyrolysis char is dusty and highly pyrophoric). The amount of water is adjusted using a design specification in order to achieve a temperature of the quenched char of 80 °C, resulting in a char slurry with about 70% water content.

3. Exergetic analysis

In contrast to energy (first law of thermodynamics), exergy shows the quality of energy in terms of obtainable work when a system is brought to thermodynamic equilibrium with its surroundings (second law of thermodynamics). In this way, an exergetic analysis reveals components that operate with relatively high inefficiencies, suggests ways to improve the overall process and fine-tune component parameters.

In the analyzed plant the kinetic and potential exergy contents of the streams are neglected and the exergy of a working fluid is assumed to be fully determined by its physical and chemical exergy. Physical exergy is the work that can be obtained when bringing a stream to the temperature

and pressure of the thermodynamic environment, while chemical exergy represents the work that can be obtained when bringing a substance or a mixture into chemical equilibrium with the surroundings. The specific chemical exergy of standard components is available in reference tables [33–35].

The exergetic analysis in this work is performed at the component level of the bio-oil generation plant. After defining the exergy of the fuel and product ($\dot{E}_P, \dot{E}_F$) of each plant component, we calculate their exergetic efficiency (ε) and exergy destruction ($\dot{E}_D$) that reveal the importance of each component in the overall structure. Incoming and outgoing streams can be part of either the exergy of the fuel or the exergy of the product of a component. The exergy destruction of component k ($\dot{E}_{D,k}$) is defined as the difference between the component's exergy of the product and fuel ($\dot{E}_{D,k} = \dot{E}_{P,k} - \dot{E}_{F,k}$), while its exergetic efficiency (ε_k) is defined as the ratio between the component's exergy of the product and fuel ($\varepsilon_k = \dot{E}_{P,k}/\dot{E}_{F,k}$). More details about the principles of exergetic analysis and the definition of exergetic efficiencies can be found in the work of Bejan et al., Tsatsaronis et al. and Frangopoulos [13,14,36].

For the purpose of this paper, we perform two simulations: The first assumes the above described plant configuration (reference), while the second – improved scenario – considers an alternative scenario where the pre-heater of the combustion air (CharCombHXC) is eliminated and the hot exhaust gases from the GCC Reactor are fed directly to the dryer. The CharCombHXC, which constitutes the difference between the two scenarios simulated, is shown in a gray shaded box in Fig. 1.

3.1. Calculating the chemical exergy of the streams

The internal database and parameter estimation system of Aspen Plus are not equipped with exergy calculations. The specific chemical exergies $\overline{e}_{ch}$ of the streams are, therefore, calculated externally. For standard components, $\overline{e}_{ch}$ is taken from existing exergy tables, based on the model of Szargut [33].

For solids and user-defined components (e.g., degraded lignin fractions), for which no tabulated values are available, the chemical exergy has been calculated depending on the property data available:

- For compounds for which the Gibbs energy of formation $\overline{g}$ is available in the Aspen Plus database or in the parameter estimation system of the software, $\overline{e}_{ch}$ is calculated via the change in the Gibbs function, according to Eq. (1) [13]:

$$\overline{e}_{ch} = -\Delta G + \left[\sum_{Prod} n * \overline{e}_{ch} - \sum_{React} n * \overline{e}_{ch}.\right] \quad (1)$$

  Here, n are the moles of each product (Prod) or reactant (React) and ΔG is the change in Gibbs Energy.
- For compounds for which $\overline{g}$ is not available, $\overline{e}_{ch}$ is calculated based on their atomic compositions and their higher heating values (HHV), using Eq. (2) [13]:

$$\overline{e}_{ch} = \overline{HHV}\,(T_0, p_0) - T_0 * \left[\overline{s}_F + \sum_{React} n * \overline{s} - \sum_{Prod} n * \overline{s}\right](T_0, p_0) + \left[\sum_{React} n * \overline{e}_{ch} - \sum_{Prod} n * \overline{e}_{ch}.\right] \quad (2)$$

  Here, $\overline{s}_F$ is the entropy of the fuel, $\overline{s}$ is the entropy of the reaction's products or reactants, and n are the moles of each product or reactant.

The chemical exergies of all compounds included in the simulation are presented in Table 1.

In order to determine the exergy content of a stream consisting of a mixture of various compounds, the concentration of each compound is taken into account. The chemical exergy of the stream is then calculated using Eq. (3) [13]:

$$\overline{e}_{ch} = \sum x_i \overline{e}_{ch,i} + \overline{R} T_0 \sum x_i ln x_i. \quad (3)$$

Here, x_i is the mole fraction of compound i in the stream at T_0, p_0, and R is the gas constant.

Table 1
Chemical exergy of compounds.

	e^{ch} (kJ/kg)	source
Environment (Air)		
N_2	24.63	[*]
O_2	124.07	[*]
Pyrolysis Gas		
CO2	451.49	[*]
CO	9821.42	[*]
CH_4	51,839.57	[*]
Ethane	49,745.84	[*]
Ethene	48,517.54	[*]
Propene	47,620.45	[*]
H_2	117,120.11	[*]
Ammonia	19,840.81	[*]
HCN	24,004.85	calc dGibbs
Water (gas phase)	527.34	[*]
Pyrolysis liquid (bio-oil)		
Water (liquid phase)	49.96	[*]
Acetic acid	15,303.36	[*]
Formic acid	6546.40	[*]
Propionic acid	20,931.62	calc dGibbs
Phenol	33,241.99	[*]
Benzene	42,292.21	[*]
Acetol	22,034.50	calc dGibbs
Acetaldehyde	26,406.84	[*]
Glycoaldehyde	17,187.05	calc dGibbs
Formaldehyde	17,931.07	[*]
Ethanedial	14,858.20	calc dGibbs
Ethenone	23,827.76	calc dGibbs
2-Propanone	29,812.40	[*]
Naphtalene	40,999.09	[*]
Xylose	14,815.75	calc HHV
Levoglucosan	17,215.03	calc dGibbs
Furfural	25,056.20	calc dGibbs
Hydroxymethylfurfural	22,389.67	calc dGibbs
Furan	31,124.50	[*]
Methanol	22,408.11	[*]
Ethanol	29,605.68	[*]
Ethylenglycol	19,451.23	[*]
Sinapylalcohol	26,159.90	calc HHV
Coumarylalcohol	31,055.88	calc HHV
Syringol	26,909.21	calc dGibbs
Degraded lignin 1 ($C_{11}H_{12}O_4$)	25,040.25	calc HHV
Degraded lignin 2 ($C_{11}H_{14}O_5$)	23,192.64	calc HHV
Degraded lignin 3 ($C_{11}H_{13}O_5$)	22,678.25	calc HHV
Pyrrolidone	27,664.16	calc dGibbs
Glutamic acid	16,265.88	[*]
Pyrrole	35,329.05	calc dGibbs
Solids		
Biomass 50% moist	9949	calc HHV
Biomass 7% moist	18,504	calc HHV
Char 0% moist	27,003	calc HHV
Char 70% moist	8027	calc HHV

"[*]": Values taken from Morris et al. [33]; "calc dGibbs": Calculations based on Gibbs Energy; "calc HHV": Calculations based on HHV.

3.2. Calculating the physical exergy of the streams

3.2.1. Gas and liquid streams

The specific physical exergy $\overline{e}^{ph}$ of a stream is calculated using its enthalpy and entropy as calculated by Aspen Plus. The physical exergy of each stream is then calculated according to Eq. (4):

$$\overline{e}_{ph} = (h - h_0) - T_0(s - s_0). \quad (4)$$

Table 2
Exergy balances for the plant with CharCombHXC (reference configuration). $\dot{E}_P$ = Exergy rate of the product; $\dot{E}_F$ = Exergy rate of the fuel; $\dot{E}_D$ (kW) = Exergy destruction rate; $\dot{E}_D$ (%) = Exergy destruction relative (contribution of the component to the overall exergy destruction); (%) = Exergetic efficiency of the component.

Component	$\dot{E}_P$ (kW)	$\dot{E}_F$ (kW)	$\dot{E}_D$ (kW)	$\dot{E}_D$ (%)	(%)
BM-dryer	69,098	76,099	7001	15.7	90.8
Mill	0	1253	1253	2.8	–
BM-cooler	–	94	94	0.2	–
PY-reactor	7194	12,555	5360	12.0	57.3
Quench	–	4221	4221	9.2	–
BO-cooler water pump	16	19	3	0.0	82.7
Cooler HXC	–	967	967	2.0	–
BO-recycle pump	5	6	1	0.0	84.3
Flue-gas compressor	295	395	100	0.2	74.7
Product gas compressor	73	98	24	0.1	75.1
Comb. air compr	5644	7257	1613	3.6	77.8
GCC-reactor	24,498	40,855	16,357	36.7	60.0
CharComb HXC	16,699	24,107	7408	16.6	69.3
Char quench	–	319	319	0.7	–
Overall plant	110,166	157,745	44,567	100	71.2

Here, h and s are the mole specific enthalpy and entropy, respectively. The subscript 0 refers to the reference environment (T_0, p_0).

3.2.2. Solid streams

As Aspen Plus does not calculate the enthalpy and entropy of solid streams, the specific physical exergy of such streams is calculated according to Eq. (5) assuming a constant solid heat capacity [37]:

$$\overline{e}_{ph} = c_p * \left[(T\text{-}T_0) - T_o \ln\left(\frac{T}{T_0}\right) - \frac{1}{\rho} * (p - p_0). \right] \quad (5)$$

Here, c_p is the specific heat capacity and ρ the density at T_0.

As all solid streams are at – or close to – atmospheric pressure, the second term of Eq. (5) can be neglected. The solid heat capacities are taken from literature:

- Biomass: The heat capacity of wood is calculated according to the linear equation $c_{p,w} = 37.2 * \text{moist} + 1{,}340$ [38]. As the temperature of the biomass streams never exceeds 100 °C, the temperature influence on $c_{p,w}$ [39] is neglected. In this way, $c_{p,w}$ is calculated to be 1,600 J/kg · K for biomass with 7% moisture and 3200 J/kg · K for biomass with 50% moisture.
- Char: The $c_{p,c}$ in this case is calculated using the best-fitting curve provided by Hankalin et al. [39]: $c_{p,c} = 1.43 + 0.355 * 10^{-3} * T - 7.32 * 10^4/T^2$. This equation results in the values of 1.5 kJ/kg · K for char at 500 °C and 0.85 kJ/kg · K at temperatures close to 100 °C.
- Ash: For ash streams a value similar to the heat capacity of sand (0.8 kJ/kg · K) is used [40,41].

4. Results and discussion

The complete exergy balances for all components in the reference configuration are presented in Table 2. The listed components are highlighted in Fig. 1 by dotted boxes.

As can be observed in Table 2, the standard process has an exergetic efficiency of 71.2%. High values of exergy destruction are found in the GCC-Reactor, the CharCombHXC, the BM-Dryer, the PY-reactor and the bio-oil recovery section (including the Quench, the Cooler-HXC and the BO Cooler Water Pump). These components account for 36.7%, 16.6%, 15.7%, 12.0% and 11.2% of the total exergy destruction within the plant, respectively (Fig. 2, left side).

4.1. Assessment of improvement potentials

Reducing the electricity consumption is a quite straightforward way to improve the exergetic efficiency of the pyrolysis plant. Compressors and pumps are responsible for about 3.9% of the total exergy destruction. Nevertheless, as these are usually well-engineered standard components, the potential for further reducing their electricity consumption (i.e., by more efficient equipment) is linked with high costs [42]. High potential for improvement is found in the mill, responsible for 2.8% of the overall inefficiencies. Reduction of the required milling energy could be achieved by increasing the screen size of the mill, but the particle size is limited by the CFB reactor technology and the use of coarser wood particles would require a different type of a pyrolysis reactor. Alternatively, the required milling energy could be reduced by more intense drying, as drier biomass is more brittle and easier to mill [24]. On the other hand, more severe drying is energy intensive and would increase the irreversibilities within the dryer, which is already the third largest source of inefficiencies in the plant.

The PY-reactor is responsible for 12.0% of the overall exergy destruction, mainly due to the chemical reactions taking place there. As the temperature range of fast pyrolysis reactors is quite limited (the bio-oil yield is maximized at temperatures around 500 °C and decreases with higher or lower reactor temperatures), there is little potential for improvement if bio-oil is the main desired product. Although the use of different reactor types would change the reaction yield and, thus, the composition of the product, it will, most probably, not change the exergy destruction due to chemical reactions in the pyrolysis process significantly. The auxiliary consumption of the given reactor type is determined by the electricity used to drive the compressor fluidizing the reactor bed. However, this compressor only causes 0.2% of the

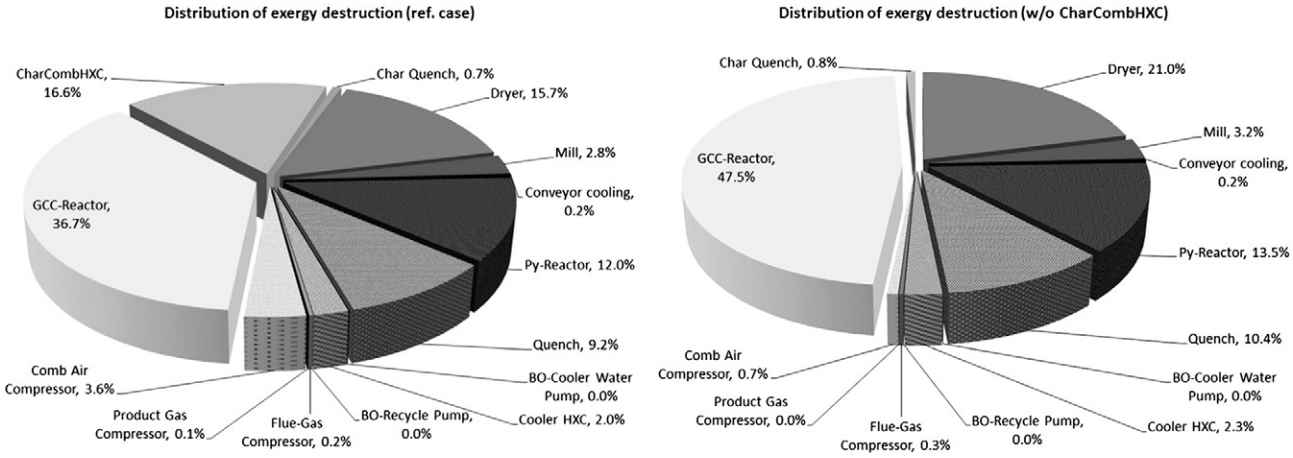

Fig. 2. Distribution of exergy destruction among the plant components; left: Reference configuration with CharCombHXC, right: Alternative configuration without CharCombHXC.

Table 3
Exergy balances for the plant without CharCombHXC. Exergy balances for the plant with CharCombHXC (reference configuration).$\dot{E}_P$ = Exergy rate of the product;$\dot{E}_F$ = Exergy rate of the fuel; $\dot{E}_D$ (kW) = Exergy destruction rate; $\dot{E}_D$ (%) = Exergy destruction relative (contribution of the component to the overall exergy destruction); (%) = Exergetic efficiency of the component.

Component	$\dot{E}_P$ (kW)	$\dot{E}_F$ (kW)	$\dot{E}_D$ (kW)	$\dot{E}_D$ (%)	(%)
BM-dryer	69,099	77,417	8317	21.0	89.3
Mill	0	1253	1253	3.2	–
BM-cooler	–	95	95	0.2	–
PY-reactor	7201	12,556	5355	13.5	57.4
Quench	–	4115	4115	10.4	–
BO-cooler water pump	16	19	3	0.0	82.9
Cooler HXC	–	915	915	2.3	–
BO-recycle pump	5	6	1	0.0	84.3
Flue-gas compressor	296	396	100	0.3	74.7
Product gas compressor	39	53	14	0.0	73.7
Comb air compr	792	1056	264	0.7	75.0
GCC-reactor	24,034	42,835	18,801	47.5	56.1
Char quench	–	309	309	0.8	–
Overall plant	108,174	147,715	39,542	100	73.2

overall exergy destruction, and hence leaves little room for improving the performance of the overall plant.

The inefficiencies within the bio-oil recovery section (Quench, CoolerHXC and BO-Cooler Water Pump) sum up to 11.2% of the total and are mainly associated with the operation of the quench cooling, which dissipates the latent heat of the pyrolysis vapors in the water-cooler (CoolerHXC) instead of using it to generate steam or to preheat the flue gases. Nevertheless, the quench cooling is required to avoid heat exchanger fouling or clogging [32] and the corresponding inefficiencies could, therefore, be characterized as unavoidable in a fast pyrolysis process.

Exergy destruction associated with chemical reactions is the principal origin of the thermodynamic inefficiencies in the GCC-Reactor. Since the GCC-Reactor provides process heat to the PY-Reactor at 520 °C, improving the exergetic efficiency by increasing the combustion temperature is not an option. Slight improvements could be achieved by further preheating the inlet streams. However, such an action would increase the air flow required by the BM-Dryer (due to the lower exhaust gas temperature) and, thus, the associated irreversibilities.

The dryer is the component that determines the air and exhaust gas flows to and from the GCC-Reactor. The exergy destruction in the dryer is high (15.7% of the total) and mainly associated with the decrease in the physical exergy of the hot exhaust gases that dry the biomass. Options to improve its performance would be to (i) reduce the temperature of the drying gas, leading to reduced exergy destruction due to the temperature drop in the dryer, or to (ii) reduce its mass flow, reducing the exergy destruction due to pressure drops. These are, however, two adverse measures, as a lower exhaust gas temperature requires a higher mass flow of drying gas.

Furthermore, due to the high mass flow of hot gas required by the dryer (and, consequently, of the combustion air for the GCC), the pressure drops in the associated components (CCAIRCMP, GCC-Reactor, CharCombHXC, Dryer) have a significant impact on the thermodynamic irreversibilities of the plant. In fact, the high exergy destruction in the CharCombHXC (16.6%) is a result of the pressure drops within this component in combination with the relatively high air flow. Taking into account that the combustion air compressor (CCAIRCMP) is responsible for another 3.6% of the total exergy destruction in the plant, reducing the drying air demand would be an efficient measure to improve the overall performance of the plant. Nevertheless, feeding the PY-Reactor with biomass of higher moisture affects the composition of the pyrolysis products and reduces the quality of the bio-oil. Thus, less intense drying is not considered a viable option.

4.2. Alternative plant configuration using a high-temperature dryer

As the CharCombHXC is identified as one of the main sources of irreversibilities in the plant, we investigate the trade-off between the exergy destruction due to pressure drops in the CharCombHXC and the temperature gradient in the BM-Dryer/the GCC Reactor by performing a simulation eliminating the CharCombHXC used to preheat the combustion air. The corresponding results are listed in Table 3, while the contribution of each component to the overall exergy destruction is visualized in Fig. 2, right side. When comparing this variation

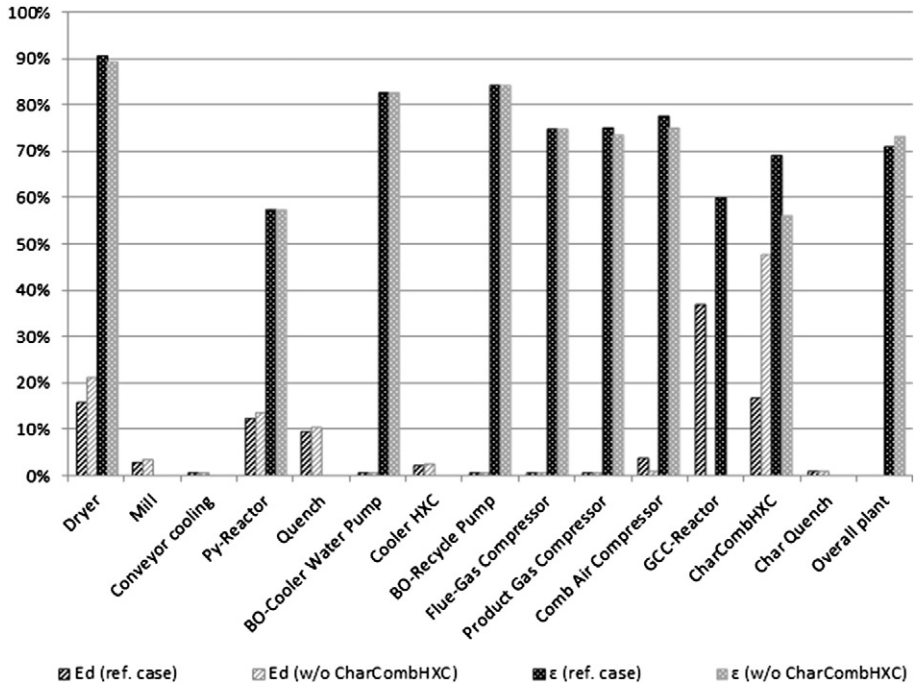

Fig. 3. Exergetic efficiencies at the component level. E_d: Relative contribution of the component to overall exergy destruction; ε: Exergetic efficiency of the component; (ref. case): Plant in the reference case configuration (with CharCombHXC); (w/o CharCombHXC): Plant in the alternative configuration (without CharCombHXC) vulnerable.

with the configuration of the reference plant (Fig. 3), it can be observed that preheating the combustion air that enters the GCC-Reactor reduces the exergetic irreversibilities in the GCC-Reactor by 12.9% (from 18,801 to 16,357 kW). At the same time, the exergy destruction in the BM-Dryer is reduced by 15.8% (from 8,317 to 7,000 kW) due to the lower temperature of the drying gases entering the dryer. Nevertheless, preheating requires a heat exchanger (CharCombHXC) that implies additional pressure drops, while at the same time colder drying gases require higher mass flows of gas in the dryer and more electricity to drive the compressors (Prod. Gas-Compressor and Comb. Air Compressor). In fact, the mass flow of the exhaust gas increases by a factor of three, and the increase in the irreversibilities in the Comb. Air Compressor and the CharCombHXC is higher than the reduction achieved in the GCC Reactor and the BM-Dryer. Hence, the thermodynamically-best configuration would be a direct-contact dryer with the uncooled exhaust gases fed directly to the BM-Dryer. This would reduce the overall exergy destruction by about 11% and increase the exergetic efficiency of the plant to 73.2% (Table 3). Nevertheless, the technical feasibility of direct-contact drying of biomass with oxygen-containing gases of 730 °C is challenging and could be associated with operational risks. Wood decomposition and volatiles release start at temperatures between 200 and 300 °C. Such high temperatures in the dryer might, hence, increase the risk of auto-ignition or explosion [43,44]. Furthermore, if a significant share of volatiles were released due to high temperatures, the higher chemical exergy lost with the exhaust gases would, once again, reduce the overall efficiency of the plant.

5. Conclusions

The pyrolysis process investigated achieves an exergetic efficiency of 71.2%, a value within the range typically found for gasification processes (between 66% and 79%) [45–48], and slightly lower than that found by Boateng et al. [15] for fast pyrolysis. However, in the present case the feedstock has a higher water content. Most exergy destruction (36.3% of the total exergy destroyed) takes place in the gas-and-char combustor and it is mainly associated with the chemical reactions taking place there. Chemical reactions are also the principal origin of irreversibilities within the pyrolysis reactor (12.0% of the total exergy destruction). Furthermore, a 9.4% of the exergy destruction is caused by the quench cooler and could be avoided if a more efficient heat recovery from the bio-oil were possible.

In the given configuration, the components with the highest potential for improvement are the biomass dryer and the mill, responsible for 15.7% and 2.8% of the total exergy destruction of the plant, respectively. The remaining components (i.e., pumps and compressors except the combustion air compressor) have a rather small influence on the overall plant performance, since their exergy destruction adds up to less than 1% of the total.

Finally, a significant improvement (an exergetic efficiency of the overall plant of 73.2%) could be achieved by eliminating the heat exchanger that preheats the combustion air with the exhaust gases of the gas-and-char combustor and feeding the exhaust gases directly to the dryer.

Acknowledgments

This research has been supported by the Regional Government of Madrid (S2009/ENE-1743) and the Spanish Ministry of Economy and Competitiveness (IPT-2012-0219-120000). Fontina Petrakopoulou would like to thank the Marie Curie Actions AMAROUT (PEOPLE-COFUND) and IEF (PEOPLE-IEF-GENERGIS-332028) funded by FP7.

Appendix A

This Appendix presents the complete stream tables used as basis for the exergy calculations of the reference configuration.

Table A1
Stream table solid streams.

Stream no.		3	7	8	9	10	23	26	49	55	56	85	86
From		DRYRSEPT	BMHOPPR	BMMILL	BMSIEVE	BMCOOLR	0	CHARCYCL	ASHCYCL	CHRSEP	CHRSEP	B1	0
To		0	BMMILL	BMSIEVE	BMCOOLR	0	1BMDECMP	0	0	CHRDCMPY	CCCHRQCH	0	DRYREACT
Temperature	K	375.0005	375.0011	375.0011	375.0011	325.0011	325.0011	793	1000	793	793	377.6687	298.5
Pressure	N/m^2	106988	101325	101325	101325	101325	101325	141855	157253	141855	141855	101325	131723
Mass flow	kg/s	8.065	13.092	13.092	8.065	8.065	8.065	1.43	0.043	0.424	1.006	3.269	15
Mass fraction													
Wood		1	1	1	1	1	1	0	0	0	0	0	1
Ash		0	0	0	0	0	0	0	1	0	0	0	0
Char		0	0	0	0	0	0	1	0	1	1	1	0
Composition													
Moisture	% (ar)	7	7	7	7	7	7	0	0	0	0	69.23759	50
Ultanal													
Ash	% (db)	1.93	1.93	1.93	1.93	1.93	1.93	10.12283	100	10.12283	10.12283	10.12283	1.93
Carbon	% (db)	50.6	50.6	50.6	50.6	50.6	50.6	73.4012	0	73.4012	73.4012	73.4012	50.6
Hydrogen	% (db)	6.08	6.08	6.08	6.08	6.08	6.08	2.6516	0	2.6516	2.6516	2.6516	6.08
Nitrogen	% (db)	0.61	0.61	0.61	0.61	0.61	0.61	0.9498889	0	0.9498889	0.9498889	0.9498889	0.61
Chlorine	% (db)	0	0	0	0	0	0	0	0	0	0	0	0
Sulfur	% (db)	0	0	0	0	0	0	0	0	0	0	0	0
Oxygen	% (db)	40.78	40.78	40.78	40.78	40.78	40.78	12.87447	0	12.87447	12.87447	12.87447	40.78

Table A2
Stream table gaseous streams.

Stream no.		1	4	5	18	20	21	47	48	50	51	57	60	61	62
From		0	DRYRSEPT	DRYHTREC	DRAIRMIX	CCAIRCMP	CCAIRHTR	ASHCYCL	EXGASCLR	PYSANDHX	PYSANDHT	0	0	BOQCHPMP	BOCOOLRC
To		CCAIRCMP	DRYHTREC	0	DRYREACT	CCAIRHTR	GASCOMB	EXGASCLR	0	0	PYSANDHX	CCCHRQCH	BOQCHPMP	BOCOOLRC	0
Temperature	K	298.5	375.0005	375.0005	600.0355	388.7699	823.2296	1000	600	774.6585	843.15	298.5	298.5	298.507	318.1021
Pressure	N/m^2	101325	106988	106988	127253	202650	172650	157253	127253	10132500	10132500	101325	101325	167186	101325
Mole flow	kmol/s	2.746527	3.19067	3.19067	2.805692	2.746527	2.746527	2.805692	2.805692	6.38347	6.38347	0.1256476	10.2593	10.2593	10.2593
Mass FLOW	kg/s	79.00616	88.02808	88.02808	81.0926	79.00616	79.00616	81.0926	81.0926	115	115	2.263577	184.8242	184.8242	184.8242
Enthalpy h-mixture	kJ/kmol	3.699001	−42226.34	−42226.34	−8364.571	2646.1	15939.79	4644.897	−8364.571	−226872	−223753.4	−285648.1	−288827.2	−288825.4	−287127.6
Enthalpy h_o-mixture	kJ/kmol	3.699001	−44531.5	−44531.5	−17463.38	3.699001	3.699001	−17463.38	−17471.52	−241829.2	−241829.2	−285648.1	−288827.2	−288827.2	−288827.2
Entropy s-mixture	kJ/kmol–K	4.040203	7.771647	7.771647	23.77298	6.007675	30.17362	38.56482	23.76818	−50.93026	−47.07154	−162.5699	−170.7471	−170.7462	−165.2325
Entropy s_o-mixture	kJ/kmol–K	4.040203	1.349992	1.349992	4.660915	4.040203	4.040203	4.660915	4.635388	−15.75797	−15.75797	−162.5699	−170.7471	−170.7471	−170.7471
Component mole fraction															
Water		0	0.1397488	0.1397488	0.0217111	0	0	0.0217111	0.0217111	1	1	1	1	1	1
N2		0.8112171	0.6984452	0.6984452	0.794281	0.8112171	0.8112171	0.794281	0.794281	0	0	0	0	0	0
Oxygen		0.1887829	0.1344566	0.1344566	0.1529058	0.1887829	0.1887829	0.1529058	0.1529058	0	0	0	0	0	0
CO2		0	0.0273213	0.0273213	0.0310701	0	0	0.0310701	0.0310701	0	0	0	0	0	0
CO		0	3.366E-12	3.366E-12	3.8279E-12	0	0	3.8279E-12	3.8279E-12	0	0	0	0	0	0
CH4		0	0	0	9.396E-46	0	0	9.396E-46	9.396E-46	0	0	0	0	0	0
Ethane		0	0	0	0	0	0	0	0	0	0	0	0	0	0
Ethene		0	0	0	0	0	0	0	0	0	0	0	0	0	0
Propene		0	0	0	0	0	0	0	0	0	0	0	0	0	0
H2		0	3.3902E-12	3.3902E-12	3.8554E-12	0	0	3.8554E-12	3.8554E-12	0	0	0	0	0	0
NO2		0	1.4781E-06	1.4781E-06	1.6809E-06	0	0	1.6809E-06	1.6809E-06	0	0	0	0	0	0
NO		0	2.6497E-05	2.6497E-05	3.0133E-05	0	0	3.0133E-05	3.0133E-05	0	0	0	0	0	0
Ammonia		0	0	0	6.2089E-21	0	0	6.2089E-21	6.2089E-21	0	0	0	0	0	0
HCN		0	0	0	3.7962E-33	0	0	3.7962E-33	3.7962E-33	0	0	0	0	0	0

Table A3
Stream table mixed streams.

Stream no.		27	28	30	31	35	36	37	38	42
From		CHARCYCL	0	B19	BOPHSSEP	BBGRCSPL	PYGASCMP	BBGRCSPL	BBFLGBLW	PYBOPMP
To		PYQUENCH	PYQUENCH	BOPHSSEP	BBGRCSPL	PYGASCMP	0	BBFLGBLW	0	0
Temperature	K	793	300.0022	299.9975	299.997	299.997	341.2136	299.997	335.3439	299.9969
Pressure	N/m^2	141855	141855	111458	111458	111458	172253	111458	162120	111458
Mole flow	kmol/s	0.4492433	2.806286	3.255638	0.3551438	0.06197385	0.06197385	0.29317	0.29317	0.094208
Mass flow	kg/s	14.70085	147.0065	161.713	9.77145	1.705153	1.705153	8.066297	8.066297	4.935059
Enthalpy h-mixture	kJ/kmol	−153518.9	−383047.6	−356725.8	−141736.6	−141736.6	−140161.1	−141736.6	−140389.5	−383049.7
Enthalpy h_o-mixture	kJ/kmol	−181222	−383253.2	−356913	−141789.9	−141789.9	−141789.9	−141789.9	−141789.9	−383253.2
Entropy s − mixture	kJ/kmol–K	24.40589	−292.5321	−260.0739	5.022525	5.022525	6.337195	5.022525	6.163819	−292.5333
Entropy s_o-mixture	kJ/kmol–K	−25.73174	−293.2117	−260.6118	5.633862	5.633862	5.633862	5.633862	5.633862	−293.2117
Component mole fraction										
Water		0.1484491	0.5688148	0.5108078	0.0370593	0.0370593	0.0370593	0.0370593	0.0370593	0.5688148
N2		0	0	0	0	0	0	0	0	0
Oxygen		0	0	0	0	0	0	0	0	0
CO2		0.1469123	0.00073606	0.0209068	0.1856437	0.1856437	0.1856437	0.1856437	0.1856437	0.00073606
CO		0.170122	6.6935E-06	0.0234809	0.2151975	0.2151975	0.2151975	0.2151975	0.2151975	6.6935E-06
CH4		0.046919	1.2488E-05	0.00648525	0.0593489	0.0593489	0.0593489	0.0593489	0.0593489	1.2488E-05
Ethane		0.00227143	4.0967E-06	0.00031698	0.00287236	0.00287236	0.00287236	0.00287236	0.00287236	4.0967E-06
Ethene		0.00675536	9.5741E-06	0.00094044	0.00854291	0.00854291	0.00854291	0.00854291	0.00854291	9.5741E-06
Propene		0.0234419	0.00010516	0.00332539	0.0296252	0.0296252	0.0296252	0.0296252	0.0296252	0.00010516
H2		0.1854229	3.6464E-06	0.0255895	0.2345521	0.2345521	0.2345521	0.2345521	0.2345521	3.6464E-06
NO2		0	0	0	0	0	0	0	0	0
NO		0	0	0	0	0	0	0	0	0
Ammonia		0.00161331	0.00054955	0.00069637	0.00189548	0.00189548	0.00189548	0.00189548	0.00189548	0.00054955
HCN		0.00831943	0.00193038	0.00281211	0.0100133	0.0100133	0.0100133	0.0100133	0.0100133	0.00193038
Aceticac		0.00855638	0.0363322	0.0324993	0.00119633	0.00119633	0.00119633	0.00119633	0.00119633	0.0363322
Formicac		0.00163342	0.00508274	0.00460676	0.00071939	0.00071939	0.00071939	0.00071939	0.00071939	0.00508274
Propncac		0.00201266	0.00899415	0.00803076	0.00016271	0.00016271	0.00016271	0.00016271	0.00016271	0.00899415
Phenol		9.7816E-05	0.00046514	0.00041446	4.8173E-07	4.8173E-07	4.8173E-07	4.8173E-07	4.8173E-07	0.00046514
Benzene		1.8923E-08	1.3356E-08	1.4124E-08	2.0401E-08	2.0401E-08	2.0401E-08	2.0401E-08	2.0401E-08	1.3356E-08
Acetol		0.00149276	0.00706927	0.00629976	1.5107E-05	1.5107E-05	1.5107E-05	1.5107E-05	1.5107E-05	0.00706927
Acetaldy		0.0586441	0.0113762	0.0178988	0.07117	0.07117	0.07117	0.07117	0.07117	0.0113762
Glycoald		0.0220449	0.1047992	0.0933798	0.00011672	0.00011672	0.00011672	0.00011672	0.00011672	0.1047992
Formaldy		0.0541757	0.00374162	0.0107011	0.0675398	0.0675398	0.0675398	0.0675398	0.0675398	0.00374162
Glyoxal		0.0140806	0.0166496	0.0162951	0.0133993	0.0133993	0.0133993	0.0133993	0.0133993	0.0166496
Keten-01		0.0112357	0.00014998	0.00167973	0.0141733	0.0141733	0.0141733	0.0141733	0.0141733	0.00014998
Acetone		0.035403	0.0110193	0.0143848	0.0418706	0.0418706	0.0418706	0.0418706	0.0418706	0.0110193
Naphtlen		0.00059724	0.00274148	0.00244559	2.9065E-05	2.9065E-05	2.9065E-05	2.9065E-05	2.9065E-05	0.00274148
Xylose		2.6693E-05	0.00012746	0.00011355	2.6098E-13	2.6098E-13	2.6098E-13	2.6098E-13	2.6098E-13	0.00012746
Levogluc		0.0157536	0.075206	0.0670021	5.1794E-09	5.1794E-09	5.1794E-09	5.1794E-09	5.1794E-09	0.075206
Furfural		2.851E-06	1.3264E-05	1.1827E-05	9.1715E-08	9.1715E-08	9.1715E-08	9.1715E-08	9.1715E-08	1.3264E-05
Hdrmtfur		0.00533479	0.0254676	0.0226894	9.8428E-09	9.8428E-09	9.8428E-09	9.8428E-09	9.8428E-09	0.0254676
Furan		9.5403E-08	2.0557E-08	3.0885E-08	1.1523E-07	1.1523E-07	1.1523E-07	1.1523E-07	1.1523E-07	2.0557E-08
Methanol		0.0069065	0.0240892	0.0217181	0.00235331	0.00235331	0.00235331	0.00235331	0.00235331	0.0240892
Ethanol		0.0037505	0.0116108	0.0105262	0.00166759	0.00166759	0.00166759	0.00166759	0.00166759	0.0116108
Etyldiol		0.00257182	0.0122688	0.0109307	2.3097E-06	2.3097E-06	2.3097E-06	2.3097E-06	2.3097E-06	0.0122688
SINPYALC		0.00166186	0.00793355	0.00706811	2.4442E-12	2.4442E-12	2.4442E-12	2.4442E-12	2.4442E-12	0.00793355
CMRYLALC		0.00324291	0.0135607	0.0121369	0.0005089	0.0005089	0.0005089	0.0005089	0.0005089	0.0135607
1MGUAIAC		0.00090482	0.00431951	0.00384832	1.4586E-11	1.4586E-11	1.4586E-11	1.4586E-11	1.4586E-11	0.00431951
1KETDM2		0.00349417	0.0166813	0.0148616	6.7005E-12	6.7005E-12	6.7005E-12	6.7005E-12	6.7005E-12	0.0166813
1KETM2		0.00290514	0.0138688	0.0123559	1.3958E-13	1.3958E-13	1.3958E-13	1.3958E-13	1.3958E-13	0.0138688
1PFET3M		8.0692E-05	0.00038521	0.00034319	2.2199E-14	2.2199E-14	2.2199E-14	2.2199E-14	2.2199E-14	0.00038521
Pyrrolid		0.00025505	0.00121744	0.00108464	3.2799E-08	3.2799E-08	3.2799E-08	3.2799E-08	3.2799E-08	0.00121744
Glutacid		7.4398E-06	3.5517E-05	3.1642E-05	4.3667E-14	4.3667E-14	4.3667E-14	4.3667E-14	4.3667E-14	3.5517E-05
Pyrrole		0.00289967	0.0126209	0.0112795	0.00032375	0.00032375	0.00032375	0.00032375	0.00032375	0.0126209

(*continued on next page*)

Table A3 (*continued*)

Stream no.		44	45	65	76	77	78	80	81	82
From		BBFGSHTR	0	BOSPLIT	BOPHSSEP	B16	B16	B18	B18	BOCOOLR3
To		1BBMIX	GASCOMB	B6	BOSPLIT	B13	B13	B19	B19	B18
Temperature	K	335.3439	341.2136	299.997	299.997	333.2858	333.2858	299.9981	299.9981	300
Pressure	N/m^2	162120	172253	111458	111458	141855	141855	111458	111458	111458
Mole flow	kmol/s	0.29317	0.06197385	2.806286	2.900494	0.4662024	2.789436	0.3551425	2.900496	3.255638
Mass flow	kg/s	8.066297	1.705153	147.0065	151.9416	13.40655	148.3065	9.771354	151.9417	161.713
Enthalpy h-mixture	kJ/kmol	−140389.5	−140161.1	−383049.7	−383049.7	−158104.7	−383677.1	−141736.7	−383049.4	−356725.4
Enthalpy h_o-mixture	kJ/kmol	−141789.9	−141789.9	−383253.2	−383253.2	−159493.3	−388511	−141790	−383253.1	−356913
Entropy s − mixture	kJ/kmol–K	6.163819	6.337195	−292.5333	−292.5333	−7.885881	−282.8192	5.023278	−292.5327	−260.0727
Entropy s_o-mixture	kJ/kmol–K	5.633862	5.633862	−293.2117	−293.2117	−9.506127	−298.1261	5.634471	−293.2116	−260.6117
Component mole fraction										
Water		0.0370593	0.0370593	0.5688148	0.5688148	0.1515373	0.5708532	0.0370628	0.5688141	0.5108078
N2		0	0	0	0	0	0	0	0	0
Oxygen		0	0	0	0	0	0	0	0	0
CO2		0.1856437	0.1856437	0.00073606	0.00073606	0.1430345	0.00049547	0.1856438	0.00073613	0.0209068
CO		0.2151975	0.2151975	6.6935E-06	6.6935E-06	0.1639194	9.2658E-06	0.2151983	6.6948E-06	0.0234809
CH4		0.0593489	0.0593489	1.2488E-05	1.2488E-05	0.0452058	1.3827E-05	0.0593491	1.249E-05	0.00648525
Ethane		0.00287236	0.00287236	4.0967E-06	4.0967E-06	0.00219156	3.6838E-06	0.00287237	4.0973E-06	0.00031698
Ethene		0.00854291	0.00854291	9.5741E-06	9.5741E-06	0.00651572	8.636E-06	0.00854293	9.5755E-06	0.00094044
Propene		0.0296252	0.0296252	0.00010516	0.00010516	0.0227074	8.603E-05	0.0296252	0.00010518	0.00332539
H2		0.2345521	0.2345521	3.6464E-06	3.6464E-06	0.178662	6.3276E-06	0.234553	3.6471E-06	0.0255895
NO2		0	0	0	0	0	0	0	0	0
NO		0	0	0	0	0	0	0	0	0
Ammonia		0.00189548	0.00189548	0.00054955	0.00054955	0.00275188	0.00035283	0.00189551	0.00054954	0.00069637
HCN		0.0100133	0.0100133	0.00193038	0.00193038	0.0126631	0.0011657	0.010013	0.00193042	0.00281211
Aceticac		0.00119633	0.00119633	0.0363322	0.0363322	0.00530776	0.0370439	0.00119638	0.0363321	0.0324993
Formicac		0.00071939	0.00071939	0.00508274	0.00508274	0.00215685	0.00501621	0.00071939	0.00508273	0.00460676
Propncac		0.00016271	0.00016271	0.00899415	0.00899415	0.0008332	0.0092337	0.00016272	0.00899414	0.00803076
Phenol		4.8173E-07	4.8173E-07	0.00046514	0.00046514	3.3813E-06	0.00048316	4.8178E-07	0.00046514	0.00041446
Benzene		2.0401E-08	2.0401E-08	1.3356E-08	1.3356E-08	3.1615E-08	1.1201E-08	2.04E-08	1.3356E-08	1.4124E-08
Acetol		1.5107E-05	1.5107E-05	0.00706927	0.00706927	0.00013479	0.00733012	1.5109E-05	0.00706926	0.00629976
Acetaldy		0.07117	0.07117	0.0113762	0.0113762	0.0820994	0.00716892	0.0711676	0.0113765	0.0178988
Glycoald		0.00011672	0.00011672	0.1047992	0.1047992	0.00115228	0.108794	0.00011674	0.1047992	0.0933798
Formaldy		0.0675398	0.0675398	0.00374162	0.00374162	0.0623053	0.00207641	0.0675388	0.00374177	0.0107011
Glyoxal		0.0133993	0.0133993	0.0166496	0.0166496	0.0313934	0.0137716	0.0133993	0.0166496	0.0162951
Keten-01		0.0141733	0.0141733	0.00014998	0.00014998	0.0111172	0.00010242	0.0141733	0.00015	0.00167973
Acetone		0.0418706	0.0418706	0.0110193	0.0110193	0.0542109	0.00772862	0.0418684	0.0110196	0.0143848
Naphtlen		2.9065E-05	2.9065E-05	0.00274148	0.00274148	9.5193E-05	0.00283842	2.9063E-05	0.00274148	0.00244559
Xylose		2.6098E-13	2.6098E-13	0.00012746	0.00012746	1.4004E-11	0.00013253	2.6105E-13	0.00012746	0.00011355
Levogluc		5.1794E-09	5.1794E-09	0.075206	0.075206	2.1326E-07	0.0782002	5.1809E-09	0.075206	0.0670021
Furfural		9.1715E-08	9.1715E-08	1.3264E-05	1.3264E-05	4.4439E-07	1.373E-05	9.1719E-08	1.3264E-05	1.1827E-05
Hdrmtfur		9.8428E-09	9.8428E-09	0.0254676	0.0254676	3.5942E-07	0.0264815	9.8456E-09	0.0254676	0.0226894
Furan		1.1523E-07	1.1523E-07	2.0557E-08	2.0557E-08	1.3183E-07	1.4014E-08	1.1523E-07	2.0558E-08	3.0885E-08
Methanol		0.00235331	0.00235331	0.0240892	0.0240892	0.0102738	0.0236308	0.0023535	0.0240892	0.0217181
Ethanol		0.00166759	0.00166759	0.0116108	0.0116108	0.00688139	0.0111353	0.00166767	0.0116108	0.0105262
Etyldiol		2.3097E-06	2.3097E-06	0.0122688	0.0122688	2.342E-05	0.0127537	2.3101E-06	0.0122688	0.0109307
SINPYALC		2.4442E-12	2.4442E-12	0.00793355	0.00793355	2.008E-10	0.00824941	2.445E-12	0.00793354	0.00706811
CMRYLALC		0.0005089	0.0005089	0.0135607	0.0135607	0.00153925	0.0139081	0.00050884	0.0135607	0.0121369
1MGUAIAC		1.4586E-11	1.4586E-11	0.00431951	0.00431951	1.0718E-09	0.00449149	1.4591E-11	0.00431951	0.00384832
1KETDM2		6.7005E-12	6.7005E-12	0.0166813	0.0166813	4.6809E-10	0.0173455	6.7022E-12	0.0166813	0.0148616
1KETM2		1.3958E-13	1.3958E-13	0.0138688	0.0138688	2.1915E-11	0.014421	1.3963E-13	0.0138688	0.0123559
1PFET3M		2.2199E-14	2.2199E-14	0.00038521	0.00038521	2.9083E-12	0.00040055	2.2207E-14	0.00038521	0.00034319
Pyrrolid		3.2799E-08	3.2799E-08	0.00121744	0.00121744	3.6436E-07	0.00126585	3.2804E-08	0.00121744	0.00108464
Glutacid		4.3667E-14	4.3667E-14	3.5517E-05	3.5517E-05	4.1835E-12	3.6931E-05	4.3683E-14	3.5517E-05	3.1642E-05
Pyrrole		0.00032375	0.00032375	0.0126209	0.0126209	0.00128161	0.0129504	0.00032376	0.0126209	0.0112795

References

[1] EC, Directive 2009-28-EC on the Promotion of the Use of Energy From Renewable Sources, European Parliament and the Council, 2009.
[2] A.V. Bridgwater, Biomass fast pyrolysis, Thermal Science 8 (2004) 21–49.
[3] R. Venderbosch, W. Prins, Fast pyrolysis technology development, biofuels, Bioproducts and Biorefining 4 (2010) 178–208.
[4] A. Bridgwater, Fast pyrolysis processes for biomass, Renewable and Sustainable Energy Reviews 4 (2000) 1–73.
[5] B.M. Wagenaar, J.H. Florijn, E. Gansekoele, R.H. Venderbosch, F.W.M. Penninks, A. Stellingwerf, Bio-oil as natural gas substitute in a 350 MW power station, 2nd World Conference and Technology Exhibition on Biomass for Energy, Industry and Climate Protection, Rome, 2004, pp. 1–11.
[6] D. Chiaramonti, A. Oasmaa, Y. Solantausta, Power generation using fast pyrolysis liquids from biomass, Renewable and Sustainable Energy Reviews 11 (2007) 1056–1086.
[7] S. Murugan, M.C. Ramaswamy, G. Nagarajan, Assessment of pyrolysis oil as an energy source for diesel engines, Fuel Processing Technology 90 (2009) 67–74.
[8] R.H. Venderbosch, A.R. Ardiyanti, J. Wildschut, A. Oasmaa, H.J. Heeres, Stabilization of biomass-derived pyrolysis oils, Journal of Chemical Technology & Biotechnology 85 (2010) 674–686.
[9] A.V. Bridgwater, Upgrading biomass fast pyrolysis liquids, Environmental Progress & Sustainable Energy 31 (2012) 261–268.
[10] L. Leible, S. Kälber, G. Kappler, S. Lange, E. Nieke, P. Proplesch, et al., Kraftstoff, Strom und Wärme aus Stroh und Waldrestholz, Karlsruhe, Germany, 2007.
[11] D. Meier, B. van de Beld, A.V. Bridgwater, D.C. Elliott, A. Oasmaa, F. Preto, State-of-the-art of fast pyrolysis in IEA bioenergy member countries, Renewable and Sustainable Energy Reviews 20 (2013) 619–641.
[12] S. Czernik, A.V. Bridgwater, Overview of applications of biomass fast pyrolysis oil, Energy & Fuels 18 (2004) 590–598.
[13] A. Bejan, G. Tsatsaronis, M. Moran, Thermal Design and Optimization, Wiley and Sons, 1996.
[14] G. Tsatsaronis, F. Czielsa, Thermoeconomics, Encyclopedia of Physical Science and Technology, V.16, 2002, pp. 659–680.
[15] A.A. Boateng, C.A. Mullen, N. Macken, L. Osgood-Jacobs, P. Carlson, Mass balance and exergy analysis of a fast pyrolysis system, ASME 2011 International Mechanical Engineering Congress & Exhibition, Denver, USA, 2011, pp. 1–6.
[16] Y. Kalinci, A. Hepbasli, I. Dincer, Exergetic performance assessment of gasification and pyrolysis processes of pre-treated wood board wastes, International Journal of Exergy 8 (2011) 99–112.
[17] F. Petrakopoulou, Comparative Evaluation of Power Plants with CO2 Capture: Thermodynamic, Economic and Environmental Performance, Technical University of Berlin, 2010. PhD Thesis.
[18] F. Petrakopoulou, G. Tsatsaronis, T. Morosuk, A. Carassai, Advanced exergoeconomic analysis applied to a complex energy conversion system, Journal of Engineering for Gas Turbines and Power 134 (2012) 031801.
[19] S.B. Jones, C. Valkenburg, C.W. Walton, D.C. Elliott, J.E. Holladay, D.J. Stevens, et al., Production of Gasoline and Diesel from Biomass via Fast Pyrolysis, Hydrotreating and Hydrocracking: A Design Case, 2009.
[20] R.P. Anex, A. Aden, F.K. Kazi, J. Fortman, R.M. Swanson, M.M. Wright, et al., Techno-economic comparison of biomass-to-transportation fuels via pyrolysis, gasification, and biochemical pathways, Fuel 89 (2010) S29–S35.
[21] H. Mullaney, I.H. Farag, C.E. LaClaire, C.J. Barrett, Technical, Environmental and Economic Feasibility of Bio-Oil in New Hampshire's North Country, New Hampshire, USA, 2002.
[22] M. Ringer, V. Putsche, J. Scahill, Large-Scale Pyrolysis Oil Production: A Technology Assessment and Economic Analysis, 2006.
[23] S. Lynch, M. Reno, Sustainable biofuels from fast pyrolysis, in: E. Technologies (Ed.), APEC Workshop on Implications of Bio-refineries for Energy and Trade in the APEC Region, Taipei, Chinese Taipei, 2009.
[24] S. Mani, A Systems Analysis of Biomass Densification Process, University of British Columbia, 2005.
[25] D. Iribarren, J.F. Peters, F. Petrakopoulou, J. Dufour, Well-to-wheels comparison of the environmental profile of pyrolysis-based biofuels, 20th European Biomass Conference and Exhibition, 2012.
[26] J.F. Peters, D. Iribarren, J. Dufour, Predictive pyrolysis process modelling in Aspen Plus, 21st European Biomass Conference and Exhibition, Copenhagen, 2013.
[27] E. Ranzi, A. Cuoci, T. Faravelli, A. Frassoldati, G. Migliavacca, S. Pierucci, et al., Chemical kinetics of biomass pyrolysis, Energy & Fuels 22 (2008) 4292–4300.
[28] T. Faravelli, A. Frassoldati, G. Migliavacca, E. Ranzi, Detailed kinetic modeling of the thermal degradation of lignins, Biomass and Bioenergy 34 (2010) 290–301.
[29] M. Calonaci, R. Grana, E. Barker Hemings, G. Bozzano, M. Dente, E. Ranzi, Comprehensive kinetic modeling study of bio-oil formation from fast pyrolysis of biomass, Energy & Fuels 24 (2010) 5727–5734.
[30] C. Dupont, L. Chen, J. Cances, J.-M. Commandre, A. Cuoci, S. Pierucci, et al., Biomass pyrolysis: kinetic modelling and experimental validation under high temperature and flash heating rate conditions, Journal of Analytical and Applied Pyrolysis 85 (2009) 260–267.
[31] E. Hoekstra, R.J.M. Westerhof, W. Brilman, W.P.M. Van Swaaij, S.R.A. Kersten, K.J.A. Hogendoorn, et al., Heterogeneous and homogeneous reactions of pyrolysis vapors from pine wood, AIChE Journal 58 (2012) 2830–2842.
[32] N. Dahmen, E. Henrich, E. Dinjus, F. Weirich, The bioliq® bioslurry gasification process for the production of biosynfuels, organic chemicals, Energy, Sustainability and Society 2 (2012) 3.
[33] D.R. Morris, J. Szargut, Standard chemical exergy of some elements and compounds on the planet earth, Energy 11 (1986) 733–755.
[34] T.J. Kotas, Exergy Method of Thermal Plant Analysis, Krieger Publishing Company, 1995.
[35] J. Ahrendts, Reference states, Energy 5 (1980) 666–677.
[36] C.A. Frangopoulos, Exergy, Energy System Analysis, and Optimization — Volume 1, EOLSS Publishers Company Ltd, 2009.
[37] A. Vosough, A. Noghrehabadi, M. Ghalambaz, S. Vosough, Exergy concept and its characteristic, International Journal of Multidiciplinary Sciences and Engineering 2 (2011) 47–52.
[38] S.A.L. Samarasekara, R.V. Coorey, Thermal capacity as a function of moisture content of Sri Lankan wood species: wheatstone bridge method, 27. Proceedings of the Technical Sessions, Institute of Physics, Sri Lanka, 2011, pp. 9–16.
[39] V. Hankalin, T. Ahonen, R. Raiko, On thermal properties of pyrolysing a wood particle, Finnish–Swedish Flame Days, Naantali, Finland, 2009, pp. 1–16.
[40] Scotash, Scotash Company Homepage, Ash Properties, 2012.
[41] M.J. Moran, H.N. Shapiro, Fundamentals of Engineering Thermodynamics, SI Version, 5th edition Wiley Interscience, 2006.
[42] F. Petrakopoulou, G. Tsatsaronis, T. Morosuk, A. Carassai, Conventional and advanced exergetic analyses applied to a combined cycle power plant, Energy 41 (2012) 146–152.
[43] W.A. Amos, Report on Biomass Drying Technology, Golden, Colorado, USA, 1998.
[44] H. Li, Q. Chen, X. Zhang, K.N. Finney, V.N. Sharifi, J. Swithenbank, Evaluation of a biomass drying process using waste heat from process industries: a case study, Applied Thermal Engineering 35 (2012) 71–80.
[45] S. Spyrakis, K.D. Panopoulos, E. Kakaras, Synthesis, modeling and exergy analysis of atmospheric air blown biomass gasification for Fischer–Tropsch process, International Journal of Thermodynamics 12 (2009) 187–192.
[46] C.C. Sreejith, C. Muraleedharan, P. Arun, Energy and exergy analysis of steam gasification of biomass materials: a comparative study, International Journal of Ambient Energy 34 (2013) 35–52.
[47] V.B. Silva, A. Rouboa, Using a two-stage equilibrium model to simulate oxygen air enriched gasification of pine biomass residues, Fuel Processing Technology 109 (2013) 111–117.
[48] Y. Wang, K. Yoshikawa, T. Namioka, Y. Hashimoto, Performance optimization of two-staged gasification system for woody biomass, Fuel Processing Technology 88 (2007) 243–250.

Nomenclature

Symbols

c	Specific heat capacity (kJ/kg · K)
$\bar{e}$	Specific exergy (kJ/kg)
$\dot{E}$	Exergy rate (kW)
ΔG	Change in Gibbs energy (kJ/kmol)
$\bar{h}$	Specific enthalpy (kJ/kmol)
$\dot{m}$	Mass flow rate (kg/s)
p	Pressure (bar)
$\bar{s}$	Specific entropy (kJ/kmol · K)
T	Temperature (°C)
y	Exergy destruction ratio (%)
x	Mole fraction
ε	Exergetic efficiency (%)
ρ	Density (kg/m^3)

Subscripts

c	Char
ch	Chemical (exergy)
D	Destruction (exergy)
F	Fuel (exergy)
i	Compound
k	Component
m	Mass
n	Amount of substance (moles)
P	Product (exergy)
p	Pressure
ph	Physical (exergy)
w	Wood
wt	Weight basis
0	Reference thermodynamic environment

Abbreviations

GCC	gas-and-char combustor
HHV	higher heating value
RCStir	continuously stirred reactor; Aspen Plus reactor type for kinetic reaction modeling assuming perfect mixing of the reactants
RGibbs	Aspen Plus reactor type that calculates the reaction products based on minimizing the Gibbs free energy
RYield	yield type reactor, Aspen Plus reactor type, black box type reactor with defined reaction yields